JOURNAL OF PROPULSION AND POWER
Vol. 21, No. 4, July–August 2005

Mission-Specific Pogo Stability Analysis with Correlated Pump Parameters

Kirk W. Dotson*
The Aerospace Corporation, Los Angeles, California 90009-2957
Sheldon Rubin†
Rubin Engineering Company, Sherman Oaks, California 91403
and
Brian H. Sako‡
The Aerospace Corporation, Los Angeles, California 90009-2957

Parameters that characterize the perturbational pressure and flow at the inlet and outlet of a pump are established through pogo stability analyses for a launch vehicle. Ground tests of the launch vehicle's engine indicate the presence of unsteady pump cavitation, and some flights of the launch vehicle exhibit frequency, amplitude, and phase locking between axial structural acceleration and engine chamber pressure—a condition emblematic of propulsion–structure interaction, or pogo. Models developed for several missions of the subject launch vehicle are used to establish the ranges of the pump parameters that yield instability during the flight pogo occurrences and stability at other times. The resulting nominal values of normalized pump cavitation stiffness and mass flow gain for the launch vehicle's engine fall into the ranges 0.62–0.86 and 0.31–0.59, respectively. These ranges account for sensitivity with respect to dynamic pump gain and to structural damping for the axial modes of the coupled launch vehicle–payload system. It is shown that cavitation stiffness is generally the predominate pump parameter when the feedline hydraulic and axial structural modes are separated in frequency. However, if the frequencies of these modes are in close proximity, mass flow gain has a strong destablizing effect.

Nomenclature

A	=	area, in.^{2}
$[B]$	=	system damping matrix
C_b	=	pump cavitation compliance $(1/K)$, in.^{2}
d	=	pump inducer tip diameter, in.
f^*	=	closed-loop frequency divided by pump rotation speed N, dimensionless
g	=	standard gravitational acceleration, in./s^2
$\bar{H}$	=	head vector from pump inlet to outlet, in.
I	=	pump inertance, s^2/in.^{2}
K	=	pump cavitation stiffness, in.$^{-2}$
$[K]$	=	system stiffness matrix
K^*	=	normalized cavitation stiffness, dimensionless
$[M]$	=	system mass matrix
$m+1$	=	dynamic pump gain, dimensionless
N	=	pump rotational speed, cps
n	=	number of inducer blades
P_s	=	steady pressure, psi
p	=	static pressure perturbation, psi
R	=	linearized pump resistance for flow perturbation, s/in.^{2}
$\bar{r}$	=	structural displacement vector at pump, in.
s	=	Laplace variable or complex frequency, s^{-1}
u_t	=	pump inducer tip velocity, in./s
$\{v\}$	=	eigenvector of system eigenmode
W_s	=	steady weight displacement, lb
w	=	weight displacement perturbation, lb
α	=	pump mass flow gain factor, s
α^*	=	normalized mass flow gain factor, dimensionless
ζ	=	coupled system (closed-loop) damping, percentage of critical
ζ_s	=	structural damping, percentage of critical
ρ	=	propellant mass density, lb-s^2/in.^{4}
σ	=	cavitation number, dimensionless
ϕ	=	flow coefficient, dimensionless

Subscripts

i	=	pump inlet
in	=	inducer inlet
j	=	pump outlet
sat	=	saturation

Received 22 March 2004; presented as Paper 2004-2027 at the AIAA/ASME/ASCE/AHS/ASC 45th Structures, Structural Dynamics, and Materials Conference, Palm Springs, CA, USA, 19–22 April 2004; revision received 24 November 2004; accepted for publication 25 November 2004.

*Senior Engineering Specialist, P.O. Box 92957-M4/911, Structural Dynamics Department. Associate Fellow AIAA.
†3531 Alana Drive. Associate Fellow AIAA.
‡Senior Engineering Specialist, P.O. Box 92957-M4/911, Structural Dynamics Department.

I. Introduction

A. Pogo Stability Background

POTENTIAL for coupling between a launch vehicle–payload structure and propulsion system is a prime consideration in the design of feed systems for liquid rocket engines. When such coupling occurs, the vehicle generally responds longitudinally in slowly varying "blossoms," as shown schematically in Fig. 1. Hundreds of oscillations may exist within a single blossom; for clarity, only a small number of oscillations are depicted in Fig. 1.

This fluid–structure interaction is called pogo (after the children's toy) and was an area of intense research beginning in 1962 (see Ref. 1). The phenomenon is typically avoided through the use of a pogo accumulator, which acts to move the frequency of the fundamental feedline hydraulic mode to below the frequency of the lowest significant coupled-system structural mode.[2]

Pogo stability analyses provide the basis for feed system design decisions.[3] The analyses are generally conducted in the frequency domain, as recommended by NASA guidelines,[2] and stability margins are assessed for the coupled propulsion–structure modes. The

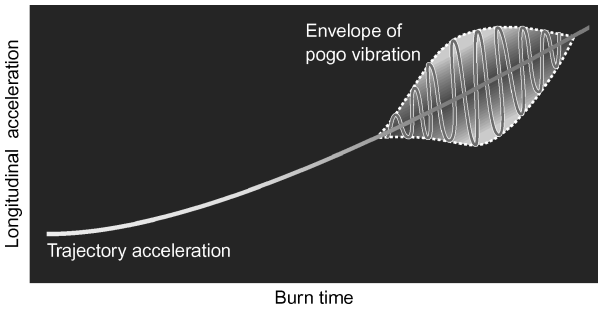

Fig. 1 Schematic of pogo response blossom in longitudinal vehicle acceleration.

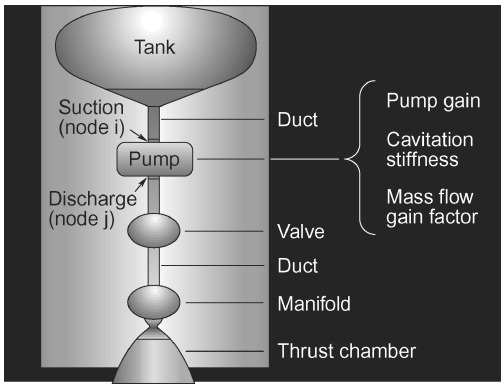

Fig. 2 Propulsion system elements for launch vehicle addressed herein (not to scale).

state variables are pressures, flows, and structural displacements at discrete points in the propulsion system.[3]

The nonlinearities that limit the pressure, flow, and structural oscillation amplitudes induced by pogo interactions are currently not well understood, and time-domain analyses that predict pogo and its amplitudes have historically been unreliable. Consequently, launch vehicle systems have traditionally been designed to preclude pogo instability, rather than to permit such interactions to occur. Moreover, the feed system is designed so that the stability of the propulsion–structure system is robust with respect to variations in the trajectory parameters, in the propellant characteristics, and in the launch vehicle and payload dynamic properties.

In pogo stability analyses, the structural dynamic model of the launch vehicle is coupled with a model of the propulsion system. The propulsion system is typically treated as an assemblage of component elements, each with one or more equations relating pressure, flow, and structural motion.[3] Figure 2 is a schematic of the elements of the propulsion system that are required for a pogo stability analysis of the launch vehicle addressed herein. Pumps, which are used to feed propellant into the thrust chamber, are generally a critical part of the propulsion system characterization.

B. Pump Cavitation

A quasi-steady bubble cloud can be produced by pump cavitation,[4] a condition typically assumed in pogo stability analysis. Additional bubbles can form intermittently. This unsteady cavitation can create local pump flow oscillations that disturb engine thrust and thus excite the vehicle structure. This excitation can affect both local pump hardware[4] and the overall launch vehicle system.[2] For example, the failure of flight No. 8 of the H-II launch vehicle is attributed to fatigue of inducer blades of the first-stage liquid hydrogen turbopump, which had a natural frequency near that of the pressure oscillations induced by unsteady cavitation.[5]

Shimura[6] reported results of tests to determine the effects of unsteady cavitation on the dynamic characteristics of the LE-7 liquid oxidizer (LOX) pump used for the H-II launch vehicle. The H-II has an accumulator in the LOX feed system, and response blossoms are not evident during H-II flight.[7] However, pogo analyses predict that the H-II first stage would be unstable without its LOX accumulator.[7]

C. Present Study

Many missions of the subject launch vehicle have exhibited low-amplitude, uncoupled oscillations during burning of the liquid rockets. However, some missions experienced self-induced oscillations, shown schematically in Fig. 1. Stability analyses conducted without unsteady pump cavitation do not account for the observed periods of pogo. That is, pogo analyses conducted with parameters for steady pump cavitation do not predict instability for the launch vehicle.

The conclusions from testing of the LE-7 LOX pump and associated analysis were of interest in the formative stage of the study reported here. The LE-7 pump exhibited rotating cavitation, attributed to periodic growth and decay of bubble pockets appearing on inducer blades supersynchronously.[6] Tests of the LE-7 pump both with and without rotating cavitation revealed that this phenomenon causes a significant difference in the dynamic pump parameters that describe the volume of cavitation bubbles during flow oscillations.

Ground tests of the subject launch vehicle's liquid rocket engine indicate the presence of unsteady cavitation at the pump inlet. The test observations led to the use of parameters in the pogo stability model that are consistent with unsteady, rather than steady, pump cavitation. However, the pump cavitation parameters could not be directly extracted from the ground test data.

The historical missions were then used to investigate if the observed unsteady cavitation explains the pogo oscillations. A pogo model was developed, and ranges of the pump parameters were established empirically, such that the periods of pogo occurrence agreed with flight experience. That is, these *flight reconstructions* yielded results consistent with pogo instability (and stability) observed during the launch vehicle missions.

Empirical values from the flight reconstructions are consistent with those for the reported unsteady cavitation phenomena on the LE-7 pump.[6] Hence, it was confirmed that the unsteady pump cavitation observed in the engine ground tests is responsible for the launch vehicle's observed pogo oscillations. It was not possible, however, to explicitly define the type of unsteady pump cavitation from the flight reconstructions.

II. Pump Modeling

A. Mathematical Development

Pumps have been modeled by using the following two equations[3]:

$$w_i - w_j = p_i/K + \alpha \dot{w}_i \tag{1}$$

and

$$p_j = (m+1)p_i - R\dot{w}_j - I\ddot{w}_j - \rho \bar{H} \cdot \dddot{\bar{r}} \tag{2}$$

The pump cavitation stiffness (K), mass flow gain factor (α), and dynamic gain ($m+1$) are assumed constant within a response cycle. They are also not motion-dependent, so that the reconstructed values presented herein are consistent with those that could be established from engine ground tests with a stationary pump.

If structural acceleration is neglected and the Laplace transform is applied, Eqs. (1) and (2) can be expressed in the form

$$\begin{Bmatrix} p_j \\ w_j \end{Bmatrix} = [T] \begin{Bmatrix} p_i \\ w_i \end{Bmatrix} \tag{3}$$

where the transfer matrix $[T]$ is defined by

$$[T] = \begin{bmatrix} (m+1) + sZ/K & -sZ(1-\alpha s) \\ -1/K & 1-\alpha s \end{bmatrix} \tag{4}$$

and the pump impedance Z is given by

$$Z = R + sI \tag{5}$$

Equations (1) and (2) are combined with those from other propulsion elements (such as feedlines, valves, tank outlets, and the thrust chamber) to form the system of coupled equations[3]

$$(s^2[M] + s[B] + [K])\{v(s)\} = 0 \tag{6}$$

where the Laplace variables s yield the frequency and damping of the coupled propulsion–structure modes.[3] Negative values of closed-loop damping indicate pogo instability or, in other words, that the coupled system response in flight will grow initially at an exponential rate.[3] Positive values of closed-loop damping indicate stability or, in other words, that the response decays from the initial conditions.

B. Dynamic Pump Gain

The pump parameters of primary interest are the dynamic pump gain, cavitation stiffness, and mass flow gain factor. Quasi-steady pump gain is defined by[3]

$$m + 1 = 1 + \partial(P_{sj} - P_{si})/\partial P_{si} \tag{7}$$

where P_{si} and P_{sj} are the steady inlet and outlet (suction and discharge) pressures.

The dynamic pump gain required in Eq. (2) generally differs from the quasi-steady value defined by Eq. (7). For example, in the test program for the first stage of the Titan II launch vehicle, dynamic pump gain based on oscillatory behavior was deduced to be significantly higher than the quasi-steady value.[2] Dynamic pump gain, consequently, is treated as a variable for pogo stability analysis.

C. Cavitation Stiffness

The stiffness K is the inverse of cavitation compliance C_b, which is defined as the sensitivity of bubble volume perturbation to pressure perturbation. A low value of K indicates a large volume change due to pressure oscillation. As shown in Eq. (1), this behavior has a strong effect on the perturbation of the propellant weight between the pump suction and discharge points.

It is known that pump cavitation stiffness is an important parameter in pogo stability analyses. Because of uncertainties in defining this variable, and because of the desire to achieve a robust and unconditionally stable propulsion system design, the cavitation stiffness is sometimes taken as the value that optimally tunes the hydraulic and structural modes to minimize system damping. This approach is not employed herein.

Pump cavitation stiffness is conventionally normalized as follows[6]

$$K^* = K\left(2\pi g d A_{\text{in}} \Big/ n u_t^2\right) \tag{8}$$

This use of the symbol K is different from that in Ref. 6, in which it denotes cavitation compliance.

D. Mass Flow Gain Factor

The pump mass flow gain factor α is the proportionality between bubble volume perturbation and incoming flow perturbation. It reflects the sensitivity of bubble volume to the angle of attack relative to the inducer blades. A positive α results when perturbational flow rate increases, so that the angle of attack at the inducer blade decreases, which in turn decreases the bubble cavity volume and, hence, increases the perturbation of propellant weight between the pump suction and discharge points.[8] (See Eq. (1).)

The experimentally determined mass flow gain factor is positive and is conventionally normalized as follows[6]:

$$\alpha^* = \alpha/(\pi d/n u_t) \tag{9}$$

System analyses have shown that increasing the mass flow gain factor tends to destabilize the coupled propulsion–structure system.

III. Flight Reconstructions

The subject launch vehicle's flight experience and the pogo stability model were used to reconstruct the values of dynamic pump gain, cavitation stiffness, and mass flow gain factor for the liquid rocket. That is, the pump parameters were allowed to vary in the pogo analysis so that the stability results agreed with instances of pogo instability (and stability) during past missions of the launch vehicle. Curves of cavitation stiffness and mass flow gain factor versus cavitation number for the LE-7 were starting points for the stability analyses.

Although there are several forms of unsteady pump cavitation, each can be modeled by choosing appropriate values of cavitation stiffness and mass flow gain factor.[4] That is, the pump model expressed by Eq. (3) is generally valid, and the empirical flight reconstruction did not require knowledge of the type of unsteady pump cavitation.

A. Procedure

Four missions of the subject launch vehicle were investigated, referred to as Missions A–D herein. Mission A exhibited three pogo response blossoms, as depicted in Fig. 3. Structural dynamic models that included a hydroelastic representation of the propellants were available for times at the beginning of each response blossom. During all three pogo occurrences, the frequency and phase of the flight acceleration and engine chamber pressure measurements "locked." That is, a sustained correlation existed between structural acceleration and engine chamber pressure. Locking of frequency and phase is common in feedback phenomena and is generally inconsistent with forced linear oscillation. A schematic depicting the locking is provided in Fig. 4.

Mission B exhibited propulsion–structure interaction for a brief time, but the frequency and phase of the flight acceleration and engine chamber pressure measurements never locked. For the purpose of the reconstruction, Mission B was assumed to be at least neutrally stable. A single structural dynamic model that included hydroelastic representation of the propellants was available for this time period. Missions C and D were used to validate the pogo stability model and did not exhibit propulsion–structure interaction.

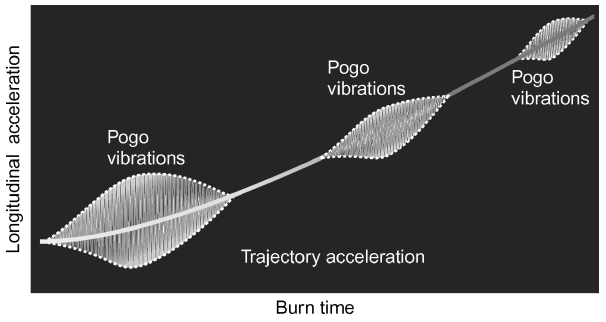

Fig. 3 Schematic of pogo response blossoms for Mission A.

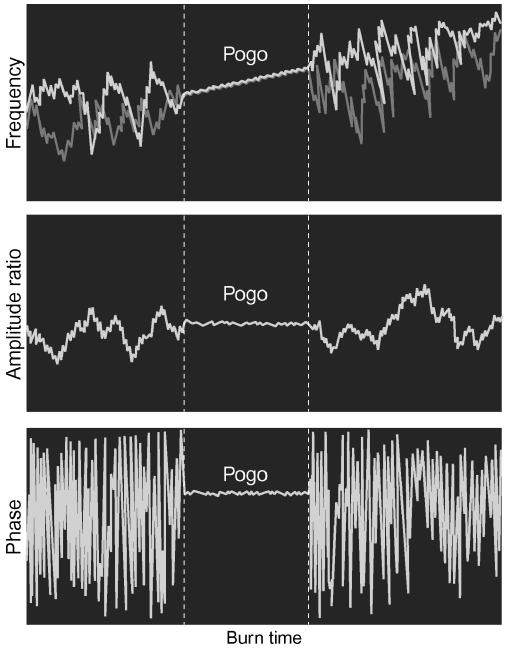

Fig. 4 Schematic of locking between oscillatory vehicle acceleration and engine chamber pressure. Pogo corresponds to the locked state.

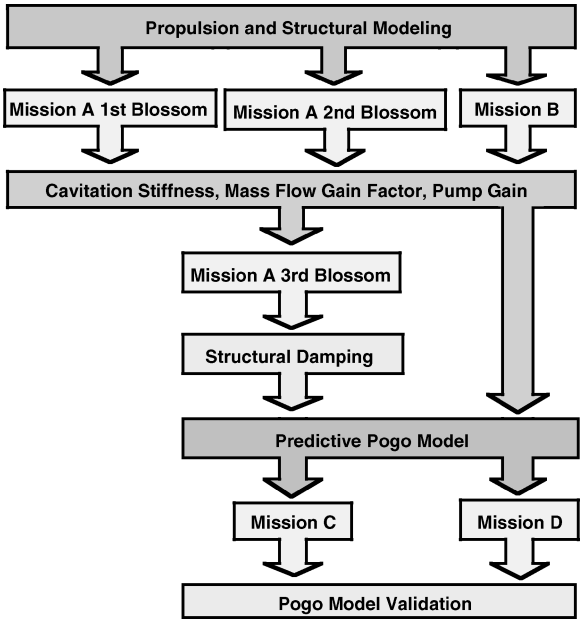

Fig. 5 Major steps in reconstruction of pump parameters and development of pogo stability model.

A flow chart indicating the major steps of the reconstruction effort is shown in Fig. 5. Values of cavitation stiffness, mass flow gain factor, and dynamic pump gain were reconstructed for engine operating conditions corresponding to Mission B and the first two blossoms of Mission A. (See Sec. III.C.) The third blossom for Mission A occurred at a different engine operating condition and was used to evaluate the effects of structural damping. (See Sec. V.B.) The resulting predictive model was validated using Missions C and D. (See Sec. VI.)

B. Unsteady Cavitation Parameters

The unsteady pump cavitation of interest here occurs in a finite region of flow coefficient (ϕ) vs cavitation number (σ) space. These two variables are defined by

$$\phi = \dot{W}_s / \rho A_i g u_t \tag{10}$$

and

$$\sigma = (p_i - p_{\text{sat}}) \Big/ \left(\rho u_t^2 / 2\right) \tag{11}$$

where the pump inducer tip speed is given by

$$u_t = \pi N d \tag{12}$$

For the engine of the subject launch vehicle, the ϕ–σ space for unsteady pump cavitation was implicitly defined from ground test and flight data.

The cavitation numbers for the first two reconstruction times for Mission A and for the single reconstruction time for Mission B were roughly equal, and, for the purpose of this study, σ was taken to be constant. The pogo stability model was, therefore, anchored based on three constraints at the average σ value, 0.042. Section V discusses verification of the model for a lower σ value.

C. Admissible K^*–α^* Regions

Figure 6 shows pump parameter values reconstructed by using the pogo stability models. For the specified dynamic pump gain values, the shaded blocks define the regions of mass flow gain factor and cavitation stiffness that yield negative and positive stability margins for Missions A and B, respectively.

The annotation on the boundaries of the region for $m+1=2.7$ also applies for the corresponding boundaries of the other regions. The annotation denotes the following:

- The pogo model for the first blossom of Mission A is unstable only for mass flow gain factor values to the right of the left boundary.

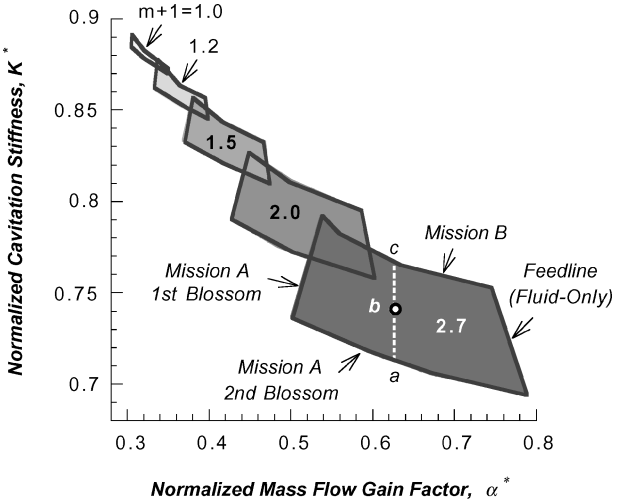

Fig. 6 Reconstruction of normalized cavitation stiffness and mass flow gain factor as a function of dynamic pump gain ($\sigma = 0.042$, $\zeta_s = 1\%$).

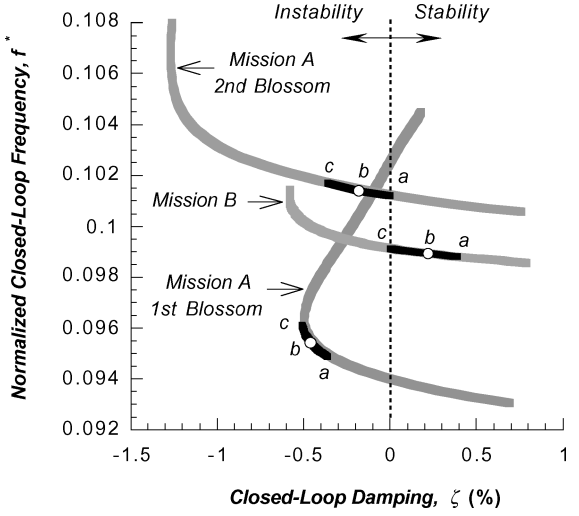

Fig. 7 K^* root loci of closed-loop frequency and damping for three flight constraints. Admissible values indicated by black lines ($\sigma = 0.042$, $m+1 = 2.7$, $\alpha^* = 0.635$, $\zeta_s = 1\%$).

- The pogo model for the second blossom of Mission A is only unstable if the cavitation stiffness is above the bottom boundary.
- The pogo model for Mission B is only stable if the cavitation stiffness is below the top boundary.
- The feedline hydraulic mode is stable for mass flow gain factor values to the left of the right boundary.

The last point requires some elaboration. The engine was tested in isolation from the launch vehicle structure. Several configurations of the feedline were used in these ground tests, but the frequency of the engine oscillations did not vary significantly between tests. Because one-dimensional instability of the feedline would have yielded different engine oscillation frequencies for the various test configurations, it can be concluded that the pogo phenomenon of interest here is not consistent with instability of the feedline hydraulic mode. Therefore, the analytical open-loop modes involving the feedline must maintain positive damping.

Closed-loop frequency and damping values are shown in Fig. 7 for $m+1=2.7$ and $\alpha^*=0.64$, which is indicated by the dashed line in Fig. 6. The plotted frequency values were normalized with respect to the pump rotational speed, N. (This normalization for frequency is not the same as that used in Ref. 6.) The black lines in Fig. 7 correspond to the admissible range of K^* shown in Fig. 6.

Note that closed-loop damping for the first blossom of Mission A is relatively insensitive to K^* over the admissible range, but that the results for Mission B and the second blossom of Mission A do vary significantly. The centers of the regions in Fig. 6 are more realistic

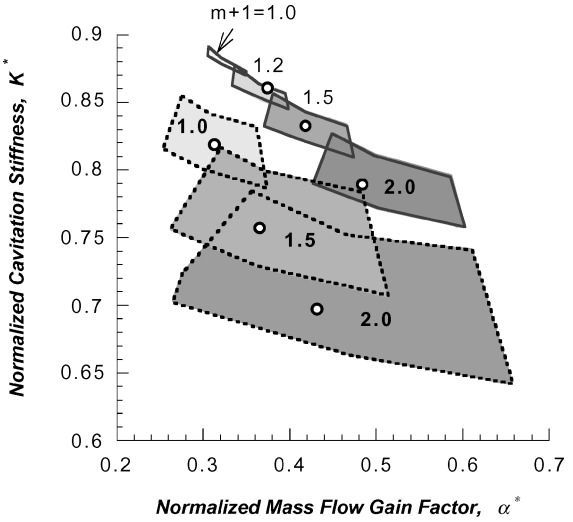

Fig. 8 Effects of structural damping on admissible values of normalized cavitation stiffness and mass flow gain factor. Open circles represent nominal K^*–α^* conditions ($\sigma = 0.042$; regions bounded by solid lines: $\zeta_s = 1\%$; regions bounded by dashed lines: $\zeta_s = 0.5\%$).

than the boundaries because the stability results that they yield are more consistent with flight observations. That is, as shown in Fig. 7, the center values simultaneously predict stability for Mission B and instability for the first and second blossoms of Mission A.

D. Effects of Structural Damping on K^*–α^* Regions

The damping values for the normal modes of the coupled launch vehicle–payload structure are approximate. Because structural damping represents the nominal condition, and because adverse propulsion–structure interaction reduces the net system damping from the nominal state, vehicle modes with low structural damping are generally more susceptible to pogo instability.

For the system addressed in the reconstructions, $\zeta_s = 1\%$ is assumed for axial modes used in the prediction of flight loads. However, mode survey tests and flight reconstructions for this system indicate that the structural damping value of the fundamental axial mode is in the range of 0.5% during periods of low-amplitude random excitation.

Figure 8 shows the effect of structural damping on the admissible K^*–α^* regions, in which $\zeta_s = 0.5\%$ and 1% have been taken as lower and upper bounds, respectively. For a given value of dynamic pump gain, a reduction in structural damping lowers the normalized cavitation stiffness and increases the size of the admissible K^*–α^* region.

The random decrement technique[9] was applied to the launch vehicle flight data to estimate system damping including propulsion–structure interaction. At the reconstruction times for the first and second blossoms of Mission A, the effective damping was approximately -0.28% and -0.08%, respectively. (Recall that negative system damping corresponds to pogo instability.)

The random decrement damping estimates are in good agreement with the exponential growth rate of the flight data amplitude at the beginning of the response blossoms. Moreover, the accuracy of the flight data does not introduce uncertainty; errors in the calibration of the flight instrumentation are negligible, and the damping estimates are not affected by time biases in the data acquisition system.

The coordinates of the open circles in Fig. 8 are provided in Table 1 and represent the unique combinations of normalized cavitation stiffness and mass flow gain factor that yield $\zeta = -0.28\%$ and -0.08% for the two Mission A reconstruction times. The open circles, therefore, may be considered the nominal K^*–α^* conditions for a given dynamic pump gain value. The positions within the region of admissible values may be considered perturbations of normalized cavitation stiffness and mass flow gain factor about the nominal conditions.

Note that when $\zeta_s = 1\%$ and $m + 1 = 1.2$, the nominal K^*–α^* condition falls on the upper boundary of the admissible region. For dynamic pump gains less than 1.2, no admissible K^*–α^* combination yields $\zeta = -0.28\%$ and -0.08% for the first and second blossoms of Mission A.

E. Admissible Dynamic Pump Gain Values

The effects of dynamic pump gain on closed-loop frequency and damping in the pogo stability analysis results are plotted in Figs. 9 and 10. The nominal K^*–α^* conditions (Table 1) were used to construct these curves.

Table 1 Nominal values of normalized cavitation stiffness and mass flow gain factor ($\sigma = 0.042$)

	K^*			α^*		
	$\zeta_s =$		Diff.	$\zeta_s =$		Diff.
$m+1$	0.5%	1%	(%)	0.5%	1%	(%)
1.0	0.82	——	——	0.31	——	——
1.2	0.80	0.86	8	0.33	0.37	12
1.5	0.76	0.83	9	0.37	0.42	14
2.0	0.70	0.79	13	0.43	0.48	12
2.7	0.62	0.73	18	0.57	0.59	4

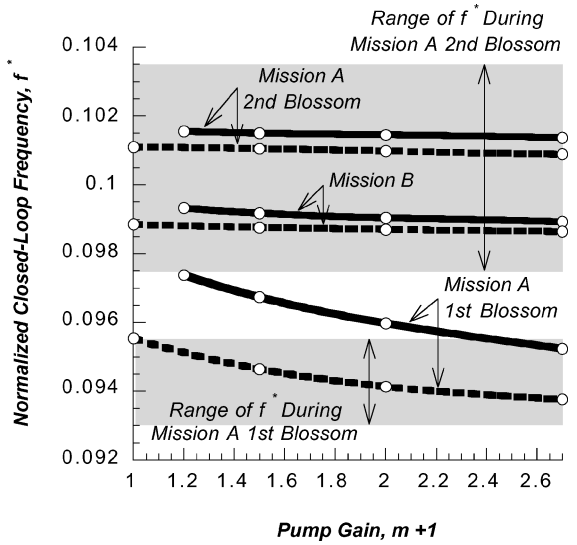

Fig. 9 Effect of dynamic pump gain on closed-loop frequency, based on nominal values in admissible K^*–α^* regions ($\sigma = 0.042$, black curves: $\zeta_s = 1\%$, dashed curves: $\zeta_s = 0.5\%$).

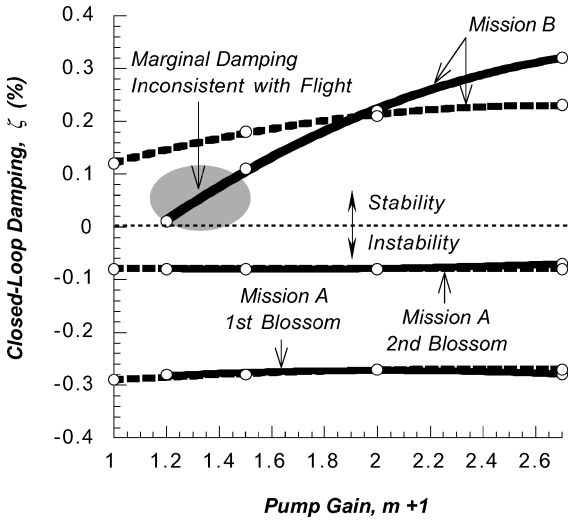

Fig. 10 Effect of dynamic pump gain on closed-loop damping, based on nominal values in admissible K^*–α^* regions ($\sigma = 0.042$, solid curves: $\zeta_s = 1\%$, dashed curves: $\zeta_s = 0.5\%$).

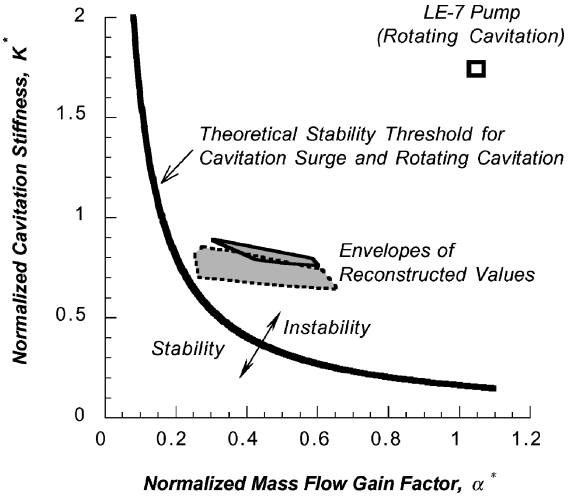

Fig. 11 Comparisons of reconstructed values with those for LE-7 pump and theory for unsteady cavitation ($\sigma = 0.042$, $\phi = 0.078$, $1 \le m+1 \le 2$, region bounded by solid lines: $\zeta_s = 1\%$, region bounded by dashed lines: $\zeta_s = 0.5\%$).

Figure 9 shows that when $\zeta_s = 1\%$ the closed-loop frequency for the first blossom of Mission A is consistent with the frequency derived from flight data for dynamic pump gain values above 2.4. Figure 10 also shows that when $\zeta_s = 1\%$ Mission B is neutrally stable for low values of dynamic pump gain. Hence, only dynamic pump gain values greater than (at least) 2 are considered admissible if the structural damping value is close to 1%.

Similarly, Figs. 9 and 10 show that when $\zeta_s = 0.5\%$ closed-loop frequency and damping for the three reconstruction times are relatively insensitive to dynamic pump gain. Hence, a broad range of dynamic pump gain values is admissible if the structural damping is close to 0.5%.

IV. Comparisons with Theory

Figure 11 compares the envelope of the admissible K^*–α^* values (Fig. 8) with the data point presented by Shimura[6] for the LE-7 pump and the test condition $\sigma = 0.041$. Also shown in Fig. 11 is the stability threshold

$$\alpha^* = 2(1+\sigma)\phi/K^* \tag{13}$$

derived by Tsujimoto et al.[8] by using a linear cascade model of the inducer and the assumption that flow perturbations downstream of the pump are negligible.

Mass flow gain factor values greater than the result of Eq. (13) yield pump instability, but not necessarily pogo instability. This theoretical stability threshold is applicable to cavitation surge and both forms of rotating cavitation (subsynchronous and supersynchronous).[8] Recall that the LE-7 pump instability is believed to be caused by supersynchronous rotating cavitation.[6]

Equation (13) is plotted in Fig. 11 using the values $\sigma = 0.042$ and $\phi = 0.078$. The flow coefficients for the three reconstruction times were roughly equal, and $\phi = 0.078$ represents the average value. The envelope of the admissible K^*–α^* values lies entirely within the region of instability for cavitation surge and rotating cavitation, which suggests that either may be the root cause of the flight pogo occurrences.

Spectra computed by using the engine ground test and flight pressure measurements exhibit numerous peaks corresponding to harmonics and amplitude modulation. It cannot be inferred that the disturbance source has a primary frequency close to that of the flight pogo occurrences. The expected frequencies for cavitation surge and rotating cavitation, therefore, cannot be used to eliminate either as the root cause of the flight pogo occurrences.

V. Cavitation Numbers < 0.042

The flight reconstructions discussed above correspond to $\sigma = 0.042$. This section addresses the values of dynamic pump gain, cavitation stiffness, and mass flow gain factor for lower cavitation numbers.

Flights of the launch vehicle addressed herein have occurred at σ values considerably lower than 0.042, without evidence of response blossoms. The lowest cavitation number at which a locking between engine chamber pressure and structural acceleration occurred (see Fig. 4) equals 0.036 and corresponds to the end of the third blossom of Mission A.

A. Cavitation Stiffness vs Cavitation Number

A relationship of pump cavitation compliance versus cavitation number was developed by using test-derived data from LOX pumps. Two sources of data were employed. One source was an average of the cavitation compliances of LOX pumps extracted from pulsing of the Saturn F-1, J-2, and H-1 engines.[6] The second source was a Shuttle 1/3-scale low-pressure oxidizer pump tested in room-temperature water at Caltech (Fig. 9.10 of Ref. 4 with a straight-line fit of points B to H). The cavitation compliances were in nondimensional form.

A relationship of cavitation compliance C_b to cavitation number σ of the following form was adopted:

$$C_b = a/(\sigma - \sigma^*)^p \tag{14}$$

This equation forces the cavitation compliance to approach infinity asymptotically as the cavitation number tends to the breakdown value σ^*. The parameters σ^*, the power p, and the factor a were determined to yield a good fit to the data. The desired outcome was a common power p and factor a for fits to the two data sources, in combination with a higher breakdown cavitation number for water than for LOX. (This upward shift in breakdown number is expected, due to the different thermodynamic effects of room-temperature water and LOX on bubble dynamics.[4])

The parameters identified were $p = 0.909$, $a = 0.074$, and $\sigma^* = 0.01$ and 0.025 for LOX and water, respectively. For the engine addressed herein, $\sigma^* = 0.01$ and $p = 0.909$; the value a was selected to pass through the anchor point defined by the pogo stability analysis for Missions A and B.

The results are shown in Fig. 12, where

$$K^* = (\sigma - \sigma^*)^p/a \tag{15}$$

The open squares in Fig. 12 are the anchor values, defined by the nominal K^* values in Table 1.

B. Third Response Blossom for Mission A

The effects of the reduction in cavitation stiffness indicated by the open circles in Fig. 12 are discussed in this section. Figure 13 shows closed-loop damping values as a function of cavitation stiffness computed by using the structural dynamic model for the third

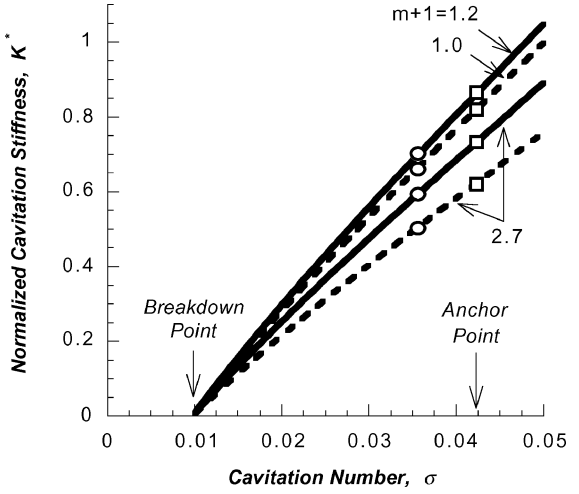

Fig. 12 Effect of cavitation number on cavitation stiffness, based on nominal K^* values for $\sigma = 0.042$ (open squares). Open circles represent K^* values at end of Mission A third blossom (solid curves: $\zeta_s = 1\%$, dashed curves: $\zeta_s = 0.5\%$).

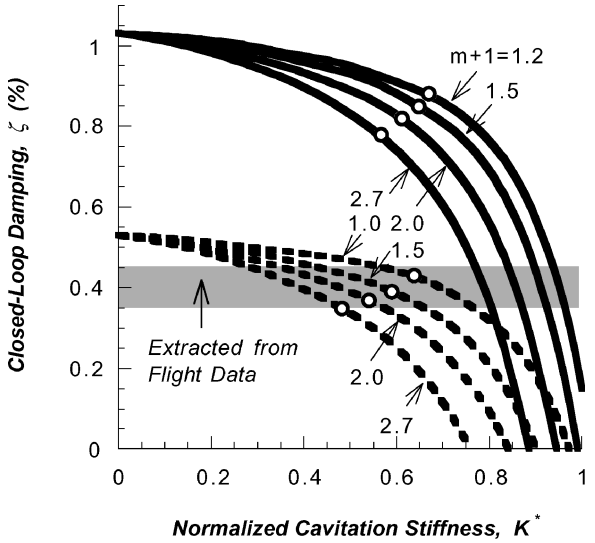

Fig. 13 Effect of cavitation stiffness on closed-loop damping for Mission A third blossom model (solid curves: $\zeta_s = 1\%$, dashed curves: $\zeta_s = 0.5\%$).

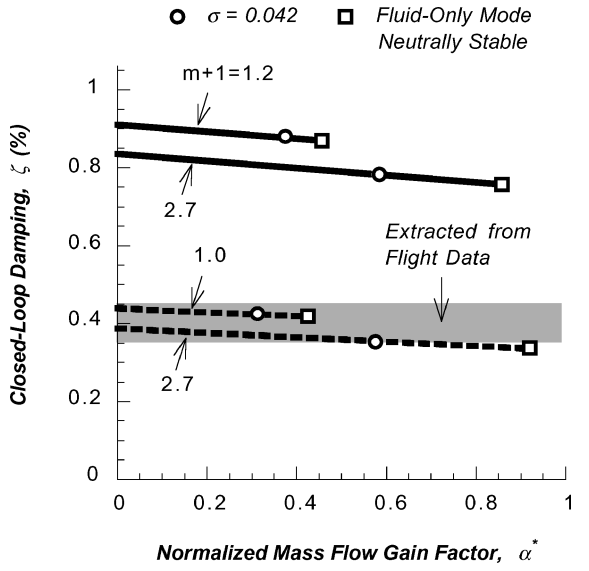

Fig. 14 Effect of mass flow gain factor on closed-loop damping for Mission A third blossom with cavitation stiffness for $\sigma = 0.036$ (solid lines: $\zeta_s = 1\%$, dashed lines: $\zeta_s = 0.5\%$).

response blossom of Mission A. The cavitation stiffness values at the end of this blossom (Fig. 12) are indicated by the open circles.

It should be noted that the hydroelastic representation of the propellants in the structural dynamic model corresponds to fill levels at the beginning of the third response blossom. The use of the structural dynamic model over the duration of the blossom consequently introduces some uncertainty into the results plotted in Fig. 13.

The random decrement technique[9] was used to extract the system damping value ($\sim$0.4%) at the end of the third blossom of Mission A. Figure 13 shows that, when $\zeta_s = 0.5\%$, this value is in good agreement with the closed-loop damping from the pogo stability analysis for all dynamic pump gain values in the range 1.0–2.7. Note that this agreement does not exist for $\zeta_s = 1\%$. Therefore, it appears that the structural damping values of the axial structural modes for Mission A are closer to 0.5% than to 1%.

The nominal mass flow gain factor values for $\sigma = 0.042$ (Table 1) were used to construct Fig. 13. Figure 14 shows the effect of mass flow gain factor over a range extending from zero to the value that destabilizes the feedline hydraulic mode. Note that the pogo stability model with $\zeta_s = 0.5\%$ yields good agreement with flight data over the entire range of mass flow gain factor.

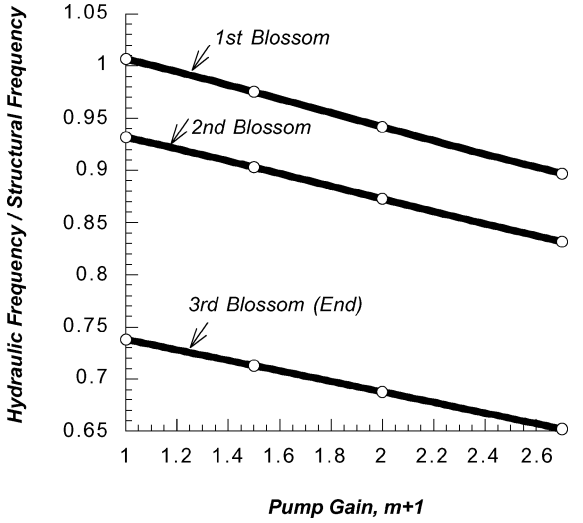

Fig. 15 Ratio of frequencies of feedline hydraulic mode and dominant structural mode for Mission A under nominal conditions ($\zeta_s = 0.5\%$).

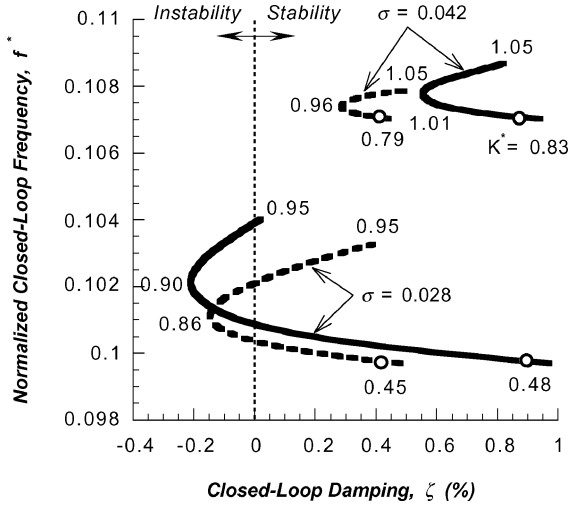

Fig. 16 K^* root loci of closed-loop frequency and damping for Mission C. Conservative predictions are indicated by open circles ($m + 1 = 2.0$; solid curves: $\zeta_s = 1\%$, $\alpha^* = 0.45$; dashed curves: $\zeta_s = 0.5\%$, $\alpha^* = 0.36$).

The reduction in cavitation number tends to stabilize the launch vehicle system because it decreases the cavitation stiffness. In physical terms, the reduced cavitation stiffness acts like a pogo accumulator and separates the natural frequencies of Mission A's structural and feedline hydraulic modes. The ratio of these frequencies is plotted in Fig. 15 as a function of dynamic pump gain under nominal conditions with $\zeta_s = 0.5\%$. Note that the frequency ratio for the end of the third response blossom is significantly lower than for the first and second blossoms.

It is evident from Figs. 14 and 15 that, when the frequencies of the structural and hydraulic modes are adequately separated, mass flow gain factor has a negligible effect on closed-loop damping. It is consequently not possible to use the structural dynamic model for the Mission A third response blossom to reconstruct mass flow gain factor for cavitation numbers less than 0.042.

VI. Further Investigations

A. Stable Missions Despite Unsteady Cavitation

As mentioned in the Introduction, many missions of the launch vehicle have flown without evidence of pogo response blossoms. Figure 16 shows root loci for Mission C, which was stable and experienced cavitation numbers 0.042 and 0.028.

Pogo stability analyses for Mission C indicate that closed-loop damping is lowest for the highest admissible K^* values. The open

circles for $\sigma = 0.042$ correspond to the peak K^* values from the boxes in Fig. 8 for $m + 1 = 2$. To define the maximum cavitation stiffness for $\sigma = 0.028$, these peak K^* values were reduced according to Eq. 15. The closed-loop damping values for the open circles in Fig. 16, therefore, represent conservative predictions for Mission C. As was the case for the Mission A third blossom mass flow gain factor had a negligible effect on the Mission C predictions, and the α^* values were taken as those commensurate with the peak K^* values in Fig. 8.

The conservative predictions (open circles) in Fig. 16 illustrate that some missions of the launch vehicle can be quite stable, even if the engine operates at conditions that produce response blossoms for other missions. The pogo phenomenon described herein, therefore, is mission-specific and depends not only on the properties of the unsteady pump cavitation but also on the modes of the coupled launch vehicle–payload structure.

B. Nominal and Conservative Conditions

The operating conditions for Mission D did not lie within the previously observed ϕ–σ space for unsteady pump cavitation, and this mission did not exhibit pogo response blossoms. In this section, a pogo model for Mission D is used to further investigate the effect of variations in cavitation stiffness and dynamic pump gain. The hypothetical engine operating point $\sigma = 0.042$ is studied to illustrate differences in the stability results under nominal and conservative conditions.

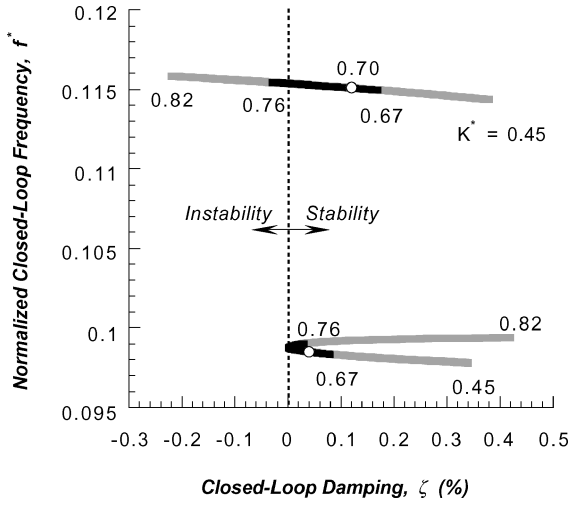

Fig. 17 K^* root loci of closed-loop frequency and damping for Mission D. Admissible values indicated by black lines. Predictions under nominal conditions indicated by open circles. $\sigma = 0.042$, $m + 1 = 2.0$, $\zeta_s = 0.5\%$, $\alpha^* = 0.43$.

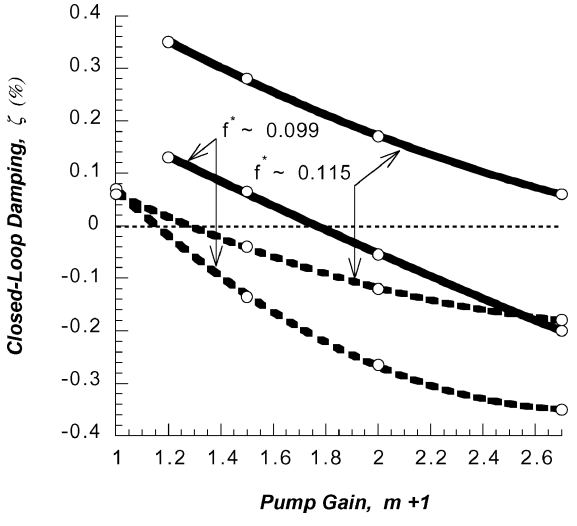

Fig. 18 Effects of dynamic pump gain on minimum closed-loop damping for Mission D. $\sigma = 0.042$; solid curves: $\zeta_s = 1\%$; dashed curves: $\zeta_s = 0.5\%$.

Root loci are shown in Fig. 17 for two coupled propulsion–structure modes of Mission D with $m + 1 = 2$. The predictions based on the nominal K^*–α^* combination (Table 1) are indicated by the open circles. The two modes shown are, therefore, marginally stable under nominal conditions.

Pogo stability analyses for Mission D indicate that the minimum value of closed-loop damping in the admissible K^*–α^* region corresponds to the upper-right corners of the boxes in Fig. 8. These minimum damping values are plotted in Fig. 18 as a function of dynamic pump gain. Note that, for all reasonable $m + 1$ values, the coupled propulsion–structure mode with $f^* \sim 0.099$ is unstable, even when structural damping is as high as 1%. Therefore, under conservative conditions, Mission D would have been unstable at the hypothetical engine operating point $\sigma = 0.042$.

VII. Conclusions

Pogo occurrences can be mission specific. That is, the dynamic properties of the spacecraft flown and the engine operating conditions of the mission design can significantly affect pogo stability margins.

A launch vehicle pogo model can be developed by reconstructing pump parameters so that the results agree with flight observations of stability and instability. The pogo model thus validated is a useful tool for stability prediction and for the selection of engine operating conditions.

Unsteady pump cavitation does not necessarily lead to significant coupling between the launch vehicle structure and propulsion system. For a pogo instability to occur, one or more of the structural modes of the coupled launch vehicle–payload system must be in close proximity to the feedline hydraulic mode.

Pump cavitation stiffness has a strong effect on the frequency of the feedline hydraulic mode and, hence, is the most significant pump parameter for inducing propulsion–structure coupling. However, once such coupling exists, the mass flow gain factor associated with unsteady pump cavitation dominates and can significantly reduce the effective system damping.

The flight reconstructions confirm that unsteady pump cavitation is responsible for the historical pogo occurrences of the launch vehicle. The resulting empirical values of cavitation stiffness and mass flow gain factor are consistent with theoretical values for rotating cavitation and cavitation surge.

References

[1]Rubin, S., "Longitudinal Instability of Liquid Rockets Due to Propulsion Feedback (POGO)," *Journal of Spacecraft and Rockets*, Vol. 3, No. 8, 1966, pp. 1188–1195.

[2]Rubin, S., "Space Vehicle Design Criteria (Structures): Prevention of Coupled Structure–Propulsion Instability (POGO)," NASA SP-8055, Oct. 1970.

[3]Oppenheim, B. W., and Rubin, S., "Advanced Pogo Stability Analysis for Liquid Rockets," *Journal of Spacecraft and Rockets*, Vol. 30, No. 3, 1993, pp. 360–373.

[4]Brennen, C. E., *Hydrodynamics of Pumps*, Concepts ETI and Oxford Science Publications, 1994, pp. 72–98, 104–107 and 247–255.

[5]Sekita, R., Watanabe, A., Hirata, K., and Imoto, T., "Lessons Learned from H-2 Failure and Enhancement of H-2A Project," *Acta Astronautica*, Vol. 48, No. 5–12, 2001, pp. 431–438.

[6]Shimura, T., "Geometry Effects in the Dynamic Response of Cavitating LE-7 Liquid Oxygen Pump," *Journal of Propulsion and Power*, Vol. 11, No. 2, 1995, pp. 330–336.

[7]Ujino, T., Shimura, T., Kohsetsu, Y., and Niitsu, M., "Pogo Prevention of H-2 Launch Vehicle," AIAA Paper 94-1624, June 1994.

[8]Tsujimoto, Y., Kamijo, K., and Brennen, C. E., "Unified Treatment of Flow Instabilities of Turbomachines," AIAA Paper 99-2678, June 1999.

[9]Ibrahim, S. R., "Random Decrement Technique for Modal Identification of Structures," *Journal of Spacecraft and Rockets*, Vol. 14, No. 11, 1977, pp. 696–700.